The generation of nearly isotropic turbulence by means of grids

P. E. Roach*

Grids have been used as a means of generating nearly isotropic turbulence for about fifty years. Even so, there does not appear to be a single document which gives adequate and simple rules for the design of such devices in an airflow installation. This paper attempts to fill this gap by means of a synthesis of experimental data with simple analyses, such that useful design guidelines are derived. Pressure losses, turbulence intensities, spectra, correlation functions and length scales are all examined. The present results are found to agree well with other data published in the literature.

Keywords: *isotropic turbulence, turbulence generation, grids*

Introduction

Paradoxically, grids are used in fluid flow studies either for the production or reduction of turbulence, and either for the creation or elimination of large-scale velocity or pressure nonuniformities. In the first dual category falls the generation of turbulence to simulate the type of conditions found in turbomachinery flow fields, and their opposite application in wind tunnels to obtain flow with very low levels of background turbulence. In the second dual category comes the production of a uniform velocity profile from nonuniform upstream conditions in a wind tunnel, and the production of a specified velocity distribution from fairly uniform upstream conditions to simulate an atmospheric boundary layer profile. The desired results are invariably accompanied by a loss of pressure across the grid. Since this pressure loss frequently limits the effectiveness of the installation, it is a factor of primary importance. Hence the ultimate goal of any general investigation must be the determination of the effects of grid geometry upon

(a) the pressure drop across the device,
(b) the characteristics of the downstream turbulence, and
(c) the modification of the time-mean velocity distribution brought about by the grid.

This paper is limited to the investigation of items (a) and (b) and to those flows where a flat, uniform-solidity grid is placed normal to a uniform stream of fluid with low background turbulence, typically with root-mean-square velocity fluctuations less than $\frac{1}{4}\%$ of the time-mean velocity. The reader interested in the performance of grids in flow streams with high background turbulence or with respect to item (c) will find Refs 1 and 2 most valuable.

A wide variety of turbulence generators have been examined in the past, including

(a) square-mesh arrays of round rods or wires (SMR),
(b) square-mesh arrays of square bars (SMS),
(c) parallel arrays of round rods or wires (PR),
(d) parallel arrays of square bars (PS),
(e) perforated plates (PP),
(f) agitated bar grids[3,4]
(g) jet grids[5,6]
(h) aerofoil cascades[7,8,9]
(i) tube bundles[10]
(j) various permutations and combinations of the above.

The present work, however, is restricted to the performance of grids of types (a) to (e) only, which are denoted by the abbreviations indicated.

* Advanced Research Laboratory Rolls-Royce plc, PO Box 31, Derby, DE2 8BJ, UK
Received 21 July 1986 and accepted for publication on 7 December 1986

The paper is presented in two parts: the first part examines the results available from the literature, and some new results are presented in the second part which both confirm and extend the existing data base.

Literature review

The simplest convenient method of generating turbulence is by means of grids of relatively large dimensions placed normal to a uniform upstream flow. Briefly, the effect of the grid on the flow field may be separated into two parts: a manipulation effect and a wake effect. The manipulation effect consists of a process whereby the spectrum of turbulence is altered, reducing or increasing the scale of the upstream turbulent eddies according to their dimensions relative to the grid. The wake effect consists of another process which contributes turbulent energy to the downstream flow field. This energy, however, is of relatively high frequency, and as a result tends to decrease the scale of the upstream turbulent eddies. Both effects interact in a complex manner to produce a downstream flow which is characterized by fairly good homogeneity and isotropy. The turbulence energy so generated is found to decay rapidly, and the eddy scales increase in size, with downstream distance. Moreover, the level of turbulence energy generated is found to be directly proportional to the pressure drop of the grid, the former being dependent upon the latter. More detailed discussion of these processes is given in Ref 1, together with some very descriptive flow visualization photographs.

Unfortunately, however, there are a number of difficulties involving both apparatus and instrumentation which introduce a variety of uncertainties in the measurements made in such flow fields. As a result of these uncertainties, poor agreement can be obtained by two or more workers using ostensibly the same experimental arrangement. Before attempting any correlation of data, therefore, it is essential that these difficulties are examined in detail in order that clear design guidelines can be determined. These problems are as follows.

(a) For a number of references, use has been made of a wind tunnel having relatively large background turbulence energy. In this case the downstream turbulence energy can be significantly increased above that which would otherwise be obtained. Some references do not quote the background turbulence characteristics, and some quote relatively large levels. The problem is not only one of relative energy levels, however, but the eddy scales can also compound the problem; one is then examining the interaction of two turbulence fields rather than the simple generation of turbulence. This problem is beyond the scope of the present work, and will not be pursued further.

(b) The turbulence characteristics of grids are usually determined by placing the grid in a duct flow of some description. This can present a further complication to the

measurements if the grid dimensions are large relative to the duct geometry. The formation and growth of the turbulence eddies will be strongly inhibited by the duct walls if the ratio of the grid to duct dimensions is significant. One might argue intuitively that the grid mesh ought to be much less than 10% of some duct dimension; this might be the duct diameter, or minimum side length should the duct be rectangular in cross-section. This argument would appear to be confirmed by some limited (unpublished) measurements by this author.

(c) Another problem associated with the duct geometry is the pressure gradient due to converging or diverging cross-sectional area. In some references a grid has been deliberately located in, or just upstream of, a slight contraction to improve the isotropy of the turbulence field. These references are not included in the present analysis.

(d) A similar problem occurs on account of the growth of boundary layers on the duct walls downstream of a grid. Not only do the boundary layers introduce a slight favourable pressure gradient, but in some instances, they can grow to a size which is a large proportion of the duct geometry. In this instance the grid turbulence can be enhanced by the boundary layer turbulence. Some references contain data which might well be contaminated by these duct boundary layers; this can be a serious problem in the quest for large distances downstream of a grid.

(e) In a number of references the importance of having tight tolerances on the mesh and diameter (or bar width) of a grid has been pointed out. Even slight deviations can have a profound influence on the downstream turbulence characteristics.

(f) Because the turbulence energy generated by a grid is directly related to its pressure loss, the sharpness of the edges of square (or rectangular) bar grids is very important. Ref 11 shows, however, that there is a maximum tolerable corner radius which does not influence the drag of square bars. This radius must be less than 5% of the bar side facing the flow.

(g) A similar problem is experienced by roughened round wires/rods used in a grid. Surface roughness can reduce the drag of circular cylinders, though the cylinder (wire) Reynolds number must usually be greater than 10^4—see Refs 12 and 13 for details. To a first approximation, the (equivalent sand) roughness must be less than 5% of the rod/wire diameter.

(h) When using hot-wires to measure turbulence properties, a systematic error is always introduced into the measurements. This is the result of the averaging of velocity variations that exist in very small distances over a much larger wire length. Turbulent flows that are convenient to deal with experimentally have small length scales of the order 0.1 mm, while typical wire lengths of 1 mm are used in practice[14]. It is only rarely that wire length corrections have been applied to grid-generated turbulence measurements. This is probably due to the uncertainties associated with the few correction schemes available rather than ignorance of the problem[15,16]. It is sufficient to note here that the errors involved in the measured turbulence intensity and length scales can be of the order 10% or more.

(i) A further systematic error is introduced into turbulence measurements when using cross-wire probes to measure two components of fluctuating velocity. When using cross-wire probes typical of those available commercially, this error can be significant and is attributed to the component of the velocity parallel to the wire[17]. This problem is addressed more fully in the Appendix, but it is sufficient here to note that the measured ratio of the turbulence energies ($\overline{u^2}/\overline{v^2}$) would be too high by a factor between 4% and 40%, depending on the details of the probe geometry.

(j) In isotropic turbulence, the micro-scale (or dissipation scale) of turbulence can be determined by means of measuring the power spectrum (see below). Moreover, it is the high frequency end of the spectrum which makes the major contribution to this length scale. It is evident that if spectra are measured over an insufficiently large frequency band, the computed micro-scale can be seriously in error, being larger than the 'true' value. Present experience (Ref 10 and some limited, unpublished results) suggests that a simple criterion can be derived for the necessary minimum frequency band. To a first approximation this minimum upper frequency f_m is given by

$$\frac{f_m \lambda_x}{U} > 5.0$$

where λ_x is the streamwise micro-length scale (see below) and U is the mean velocity of the flowstream. It is suspected that some references have not satisfied the above criterion. Note, however, that the above inequality is only to be used as a rough guideline at the present time, which would give an error less than 1% in the measured value of λ_x.

(k) The final uncertainty considered here is associated with reading data points off the small-scale graphs which are often included in certain publications. This can be a serious problem for which there is often no solution.

The above is a list of the major sources of random and systematic errors and uncertainties associated with the measurement of turbulence downstream of grids. It is by no means complete, but merely highlights some of the more serious problems. Because of these, some of the references to grid turbulence available in the literature have been rejected from the present analysis. Also, from the above list it is clear that a statistical analysis of grid turbulence is necessary, comparing the large numbers of available data sets. The data are examined with reference to available analyses, though the derivations of the formulae used are omitted since these are readily available in the primary references cited.

There are two final points which must be made before examination of the literature can proceed. The first is that there is an initial distance in the immediate wake region downstream of a grid where the flow is strongly inhomogeneous. This 'set-up'

Notation

d	Wire/rod diameter or bar width of grid
d_e	Effective value of d for perforated plates
D	Hole diameter of perforated plates
$E(f)$	One-dimensional power spectral density
f	Frequency
$f(x)$	Coefficient of spatial, longitudinal correlation
g	$(M-d)$
$g(y)$	Coefficient of spatial, lateral correlation
k	Hot-wire yaw correction factor
M	Mesh length of grid
$R(T)$	Autocorrelation function
R_d	Reynolds number $\equiv Ud/\nu$
t	Time; Plate thickness for perforated plates
T	Time delay
Tu, Tv, Tw	x-, y-, z-components, respectively, of turbulence intensities
$\overline{u^2}, \overline{v^2}, \overline{w^2}$	x-, y-, z-components, respectively, of mean square fluctuating velocities
U	Mean flow velocity
x, y, z	Streamwise and normal Cartesian coordinates
α	Hot-wire inclination (yaw angle)
β	Grid porosity
$\Delta p/q$	Pressure loss coefficient
$\lambda_x, \lambda_y, \lambda_z$	x-, y-, z-components, respectively, of dissipation or microscales
$\Lambda_x, \Lambda_y, \Lambda_z$	x-, y-, z-components, respectively, of integral length scales
ν	Fluid kinematic viscosity

phase is a result of the initially isolated bar wakes growing in size and eventually coalescing into a truly homogeneous turbulent flow. Examination of the experimental evidence shows that this wake region scales on the grid mesh size, and that the flow may be considered homogeneous by ten mesh lengths downstream of the grid. This wake region is of no interest to the present work, and consequently data obtained at smaller downstream distances will not be considered in the remainder of this paper.

The second point to be considered is that several workers have found flow instabilities when grid solidity has been sufficiently large. The evidence suggests that significant flow instability might ensue for grid solidities greater than 50%. This evidence is not conclusive, however, and this author wonders whether the problem is in actuality one of large grid dimensions relative to the duct in which the grid is located. Nevertheless, the use of grids with solidity greater than 50% is not recommended.

Pressure losses

Considerable attention has been given to correlating the pressure loss associated with round wire/rod grids, and excellent reviews will be found in Refs 18 and 19. Numerous correlation parameters have been suggested over the years with varying degrees of success. There now appears to be clear evidence that one method in particular is superior to the others, and this is outlined here.

Following the work of Ref 18, for incompressible flow the pressure drop Δp of grids is well correlated by the equation

$$\frac{\Delta p}{q}=A\left(\frac{1}{\beta^2}-1\right)^B \tag{1}$$

where q is the upstream dynamic pressure and β is the grid porosity. A and B are functions of Reynolds number, Mach number and grid geometry, whose values are given below. Although this paper is primarily concerned with truly incompressible flow, some indication of the influence of Mach number is given in Refs 18 and 19. The only comment made here is that in some references the influences of Reynolds and Mach number appear to have been confused, hence some care must be taken in the interpretation of the correlations presented in the above references.

Comparison of Eq (1) with the experimental data is given below.

Turbulence energy

As with the pressure losses, numerous experiments have been conducted over the years to determine the downstream turbulence characteristics of grids. Several theoretical treatments have also been presented, notably the methods of Batchelor[20] and Frenkiel[21]. Moreover, there have been previous attempts to combine the wealth of experimental data with theory, for example Naudascher and Farell[22]. However, there would appear to be no single document which gives adequate design guidelines for the choice of grid to give a specified turbulence field.

Having analysed the theoretical treatments of Refs 20, 21 and 22, the method due to Frenkiel would appear to give best agreement with available experimental results. Briefly, Frenkiel shows that for high Reynolds number flows (ie above those where viscous effects are significant),

$$Tu=C\left(\frac{x}{d}\right)^{-5/7} \tag{2}$$

where Tu is the streamwise component of the turbulence intensity, x is the distance downstream of the grid, and d is the representative grid dimension. Frenkiel suggests the rod/wire diameter or bar width is the appropriate dimension, and this is confirmed by the data presented below. The 'constant' C is a function of grid geometry and possibly Reynolds number, and also reflects the drag force experienced by the individual (isolated) elements of the grid—see below for details. The method of Frenkiel has the added attraction that it is not necessary to estimate the grid pressure loss in order to compute the downstream turbulence energy, unlike the methods of Refs 20 and 22.

The components of turbulence intensity may be defined by

$$Tu=\frac{\sqrt{u^2}}{U}$$

$$Tv=\frac{\sqrt{v^2}}{U}$$

$$Tw=\frac{\sqrt{w^2}}{U}$$

where $\sqrt{u^2}$, $\sqrt{v^2}$ and $\sqrt{w^2}$ are the fluctuating velocity components in the streamwise and two normal directions, respectively. Now, if the turbulence is truly isotropic all three components are equal: this has generally been found to be untrue in grid-generated turbulence, and so all three components are examined in the fourth section. The available experimental data are examined in relation to the formulae

$$Tv=DC\left(\frac{x}{d}\right)^{-5/7} \tag{3}$$

and

$$Tw=EC\left(\frac{x}{d}\right)^{-5/7} \tag{4}$$

where D and E are constants of the order 1.

Power spectra and correlation functions

It would be over-simplistic to consider only the turbulence energy generated by a grid, since this energy is spread over a broad frequency band. The whole spectrum of energy must therefore be examined in order that a more complete understanding may be gained. Numerous relationships can be determined for the energy spectra and correlation functions of all three components of the velocity fluctuations in a turbulence field. A thorough analysis is out of the scope of the present work; Ref 15 will be found most useful in this respect. Instead, only a few examples are considered here as they will be of use in later sections of this paper.

Consider, for instance, the streamwise component of the velocity fluctuations at a fixed point in the flow field, and that the turbulence is statistically homogeneous and isotropic with respect to time. Then, denoting by $E(f)$ the energy within a small frequency band $\mathrm{d}f$, the turbulence energy is defined by

$$\overline{u^2}=\int_0^\infty E(f)\,\mathrm{d}f$$

In practice, the integral need not be taken over an infinite frequency band, since above a certain frequency (typically 10–100 kHz) the energy content is negligible. Now, if the turbulence is truly homogeneous and isotropic, it is possible to fit the power spectrum with the simple relationship (Ref 15, p 60)

$$\frac{4\overline{u^2}\,\Lambda_x}{E(f)U}=1+\left(\frac{2\pi f\Lambda_x}{U}\right)^2 \tag{5}$$

where Λ_x is the streamwise component of the eddy integral length scale (see below).

Further information can be gained by considering the correlation between the streamwise velocity fluctuations at a fixed point in the flow at two different instants in time, t and $t-T$. This gives the autocorrelation function $R(T)$, defined by

$$R(T)=\frac{\overline{u(t)u(t-T)}}{\overline{u^2}}$$

where the overbar denotes the time-mean value. As with the

power spectrum, a simple formula may be used to define the autocorrelation to a first approximation:

$$R(T)=\exp(-UT/\Lambda_x) \tag{6}$$

It must be emphasized that Eqs (5) and (6) only apply to strictly homogeneous, isotropic turbulence in a uniform velocity flow field, and even then they do not apply to very high frequencies or very small time delays. Nevertheless, they can be compared with experimental data to give some indication of the degree of isotropy obtained by means of grids.

Two other frequently determined correlation functions can be defined which help to describe a homogeneous turbulent flow. These are the longitudinal and lateral coefficients of spatial velocity correlation, $f(x)$ and $g(y)$, respectively. From Ref 15 their definitions are

$$f(x)=\frac{\overline{u(x)u(x+\Delta x)}}{\overline{u^2}}$$

and

$$g(y)=\frac{\overline{u(y)u(y+\Delta y)}}{\overline{u^2}}$$

where Δx and Δy denote increments in the x and y directions, respectively. These functions can be determined by measuring the correlation between two single hot-wire outputs (normal to the flow) with varying probe separation. Moreover, assuming the validity of Taylor's hypothesis (Ref 15, p 40), the two correlation functions $R(T)$ and $f(x)$ are found to be equivalent.

Turbulence length scales

Turbulence length scales can be determined which provide further information regarding the properties of a turbulent fluid flow. Two of the more commonly quoted length scales are discussed here; other scales are described fully in Ref 15, p 184f.

The dissipation- or micro-scale λ may be considered a measure of the average dimensions of the eddies which are mainly responsible for the dissipation of turbulence energy. By definition, the streamwise micro-scale λ_x is given by,

$$\frac{1}{\lambda_x^2}=\frac{-1}{2U^2}\left\{\frac{\partial^2 R(T)}{\partial T^2}\right\}_{T=0} \tag{7}$$

Alternatively, if the turbulence field is considered truly homogeneous and isotropic it is possible to determine this micro-scale from the power spectrum. Thus,

$$\frac{1}{\lambda_x^2}=\frac{2\pi^2}{U^2\overline{u^2}}\int_0^\infty f^2E(f)\,\mathrm{d}f \tag{8}$$

In a similar manner it is possible to determine the two normal components of the micro-scale, λ_y and λ_z (Ref 15). Note, however, that for truly isotropic turbulence,

$$\lambda_y\equiv\lambda_z=\lambda_x/\sqrt{2} \tag{9}$$

From theoretical considerations[15,21] it is possible to derive a relationship between the micro-scale and the turbulence decay rate. Thus,

$$\frac{\mathrm{d}\overline{u^2}}{\mathrm{d}t}=-10\nu\frac{\overline{u^2}}{\lambda_y^2}$$

Since $t=x/U$ and $\overline{u^2}=(UTu)^2$, and noting Eq (9) above, this equation can be re-arranged to give

$$\left(\frac{\lambda_x}{d}\right)^2=\frac{-10Tu}{R_d\{\mathrm{d}Tu/\mathrm{d}(x/d)\}} \tag{10}$$

Combining Eq (10) with Eq (2) gives

$$\left(\frac{\lambda_x}{d}\right)^2=\frac{14F(x/d)}{R_d} \tag{11}$$

where F is a constant which equals 1 for truly isotropic turbulence. Similarly, through Eq (9),

$$\left(\frac{\lambda_y}{d}\right)^2=7G(x/d)/R_d \tag{12}$$

$$\left(\frac{\lambda_z}{d}\right)^2=7H(x/d)/R_d \tag{13}$$

Note that the empirical constants F, G and H have been added here merely for convenience in analysing the data: they should be approximately equal, with a value of 1 if the turbulence is truly isotropic. This is discussed further in a later section.

There is another length scale besides the micro-scale that is important in defining the structure of turbulence. The integral- or macro-scale Λ may be considered a measure of the largest eddy size in a turbulent fluid. The streamwise component of the integral scale Λ_x is defined by

$$\Lambda_x=U\int_0^\infty R(T)\,\mathrm{d}T \tag{14}$$

Assuming the turbulence can be considered truly homogeneous and isotropic, it is also possible to determine this integral scale from the power spectrum. Thus, from Eq (5) it is seen that as $f\to 0$,

$$\Lambda_x=\left[\frac{E(f)U}{4\overline{u^2}}\right]_{f\to 0} \tag{15}$$

In a similar manner[15] it is possible to determine the two normal components of the integral scale, Λ_y and Λ_z. Note, however, that for truly isotropic turbulence,

$$\Lambda_y\equiv\Lambda_z=\Lambda_x/2 \tag{16}$$

It is not possible to derive a rigorous theoretical treatment for the growth rate of the integral scales. The approach adopted here is to simply assume that the integral scales grow at a rate which is proportional to the growth rate of the micro-scales. This assumption would appear to be reasonable on intuitive grounds, and indeed Ref 15, p 53 would appear to confirm this. Moroever, Ref 15 suggests that, to a first approximation,

$$\Lambda_x/\lambda_x\approx O(\Omega(\pi/2)^{1/2}) \tag{17}$$

A further empiricism is necessary, however: both the present data and those in the literature appear to show no Reynolds number dependence for the integral length scales (over the range $10^2<R_d<10^4$). Therefore, combining Eqs (11), (12), (13), (16) and (17) and removing the Reynolds number dependence gives

$$\Lambda_x/d=I(x/d)^{1/2} \tag{18}$$

$$\Lambda_y/d=\frac{IJ}{2}(x/d)^{1/2} \tag{19}$$

$$\Lambda_z/d=\frac{IK}{2}(x/d)^{1/2} \tag{20}$$

Again, empirical constants (J and K) have been added for convenience in analysing the data: they, too, ought to be approximately equal, with a value of 1 if the turbulence is truly isotropic. See below for further discussion.

Present experimental arrangements

The present experimental work was initiated to both confirm and extend the existing data base. To achieve this aim, two air flow facilities were used: one was of small scale known as the turbulence rig, the other a larger scale wind tunnel. These facilities and the instrumentation used are described below.

The turbulence rig has been designed to present a uniform, steady and filtered airflow to a small working section, with a moderately low turbulence level. The present experiments were performed at around 30 m/s, will background streamwise turbulence intensity and integral length scale of 0.45% and

15 mm, respectively. The working section is made of Perspex and is 50 mm by 76 mm in section by 610 mm in length. Grids of a wide variety of types can be located at the upstream end of the working section. Further details are given in Ref 10, together with a scale diagram of the facility.

Due to the relatively high turbulence level of the turbulence rig, further experiments were performed using an open-return wind tunnel with a much lower background turbulence intensity. The present experiments were performed at around 10 m/s, with background streamwise turbulence intensity and integral length scale of 0.1% and 6.1 mm, respectively. The working section is 2 m long with a section of 710 mm by 260 mm.

For all the turbulence measurements, a single hot-wire probe was used (5 μm diameter, 1.25 mm sensing length) oriented normal to the flow direction. This was coupled to a standard (55D and 55M series) DISA constant-temperature anemometry system. Power spectra and autocorrelation measurements were made by means of a Hewlett-Packard HP5420 spectrum analyser and the bulk of the data were recorded on cassette tapes and analysed via an HP9825 desk-top computer.

A range of grid types and sizes have been examined, and their principal dimensions are given in Table 1. Note that the wire gauze and perforated plates used are a standard, commercially available type. Since perforated plates have a physically different geometry to the other grid types considered here, a very simple (yet effective) means has been devised to relate the two geometries. When considering the downstream turbulence properties of grids, it is found that the appropriate nondimensionalizing length scale is the wire/rod diameter or bar width, d. Thus, an effective bar width, d_e, may be defined when considering perforated plates. Moreover, the perforated plates more nearly resemble the square-mesh array grid rather than the parallel array. Now, the porosity β of a square-mesh grid is given by

$$\beta = (1 - d/M)^2 \tag{21}$$

where M is the mesh length—see sketch accompanying Table 1. Furthermore, if $M = g + d$, g being the gap between rods, then Eq (21) can be rewritten

$$\frac{d}{g} = \frac{1}{\beta^{1/2}} - 1$$

Table 1 Principal grid dimensions in present work

Grid type	Installation	M (mm)	d (mm)	t (mm)	D (mm)	β
PR	Turbulence rig	7.14	2.96	—	—	0.585
PS	Turbulence rig	7.17	2.84	—	—	0.603
PP	Turbulence rig	2.84	—	1.59	1.59	0.284
PP	Turbulence rig	4.05	—	0.50	1.40	0.108
PP	Turbulence rig	8.65	—	1.53	4.75	0.273
SMR	Wind tunnel	4.23	0.914	—	—	0.615
PR	Wind tunnel	25.4	6.35	—	—	0.750
PS	Wind tunnel	25.4	9.53	—	—	0.625

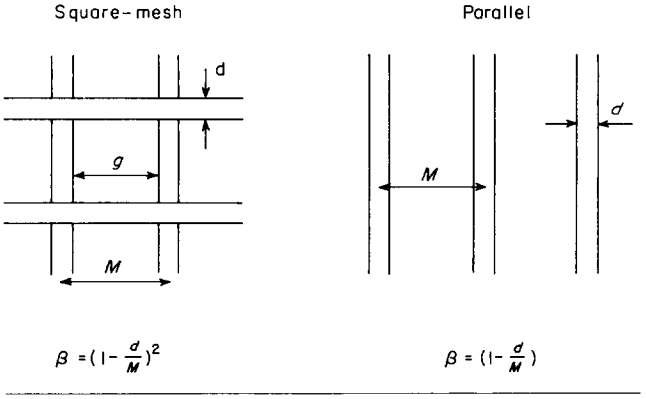

Table 2 Summary of empirical constants

Constant	Grid type: SMR	SMS	PR	PS	PP	Equation
A	0.52	0.98	0.52	0.98	0.94	1
B	1.00	1.09	1.00	1.09	1.28	1
C	0.80	1.13	0.80	1.13	1.13	2
D	←		0.89		→	3
E	←		0.89		→	4
F	←		1.21		→	11
G	←		1.21		→	12
H	←		1.21?		→	13
I	←		0.20		→	18
J	←		1.00		→	19
K	←		1.00?		→	20
Figure symbols:	○	△	□	▽	◇	

Open symbols denote present data
Filled symbols denote literature data
NB: See text for limitations to these figures

Finally, replacing d with d_e and making the further assumption that g is equivalent to the hole diameter D for the perforated plates, the simple relationship

$$\frac{d_e}{D} = \frac{1}{\beta^{1/2}} - 1 \tag{22}$$

is derived. Eq (22) has been used in the final analysis, below, when considering the turbulence characteristics of perforated plates. Moreover, each of the three perforated plates tested by this author has consisted of a hexagonal array of circular holes.

All of the present experimental turbulence data have been corrected for the influence of finite hot-wire length by the method given in Ref 15. For the turbulence rig experiments, these corrections were of the order 10% for the intensity and length scale measurements, whereas in the wind-tunnel these corrections were only 1% to 2%.

Synthesis of analysis with experiment

The equations used to define the fluid dynamics of grids having been outlined, in this section the present data, together with that available in the literature, is combined with the analysis outlined in the literature review, above. The constants of proportionality are determined for each property in turn, and are summarized in Table 2.

Pressure losses

Starting with the square-mesh arrays of round wires/rods (SMR), it is found that Eq (1) is most satisfactory with B set equal to 1. The remaining 'constant', A, is found to be strongly dependent on Reynolds number, as shown in Fig 1. Here, the Reynolds number $R_d = Ud/\nu$ where U and ν are the upstream fluid velocity and kinematic viscosity, respectively, and d is the wire/rod diameter. The data (taken from Refs 1, 18 and 23 to 37) are seen to be rather scattered, but a fair mean line can be fitted, as indicated. Note that, although shown over a wide dynamic range, the usual practical operating Reynolds number range is between 10^2 and 10^4.

Much less data are available for the parallel array grids comprising round wire/rods (PR) (see Fig 1). However, it is suggested here that the pressure drop of a PR grid is approximately equal to that for an SMR grid having the same porosity and operating at the same Reynolds number (from Refs 5, 38 and present work). This tentative suggestion needs further experimental verification, especially at Reynolds numbers outside the (limited) range examined in Fig 1.

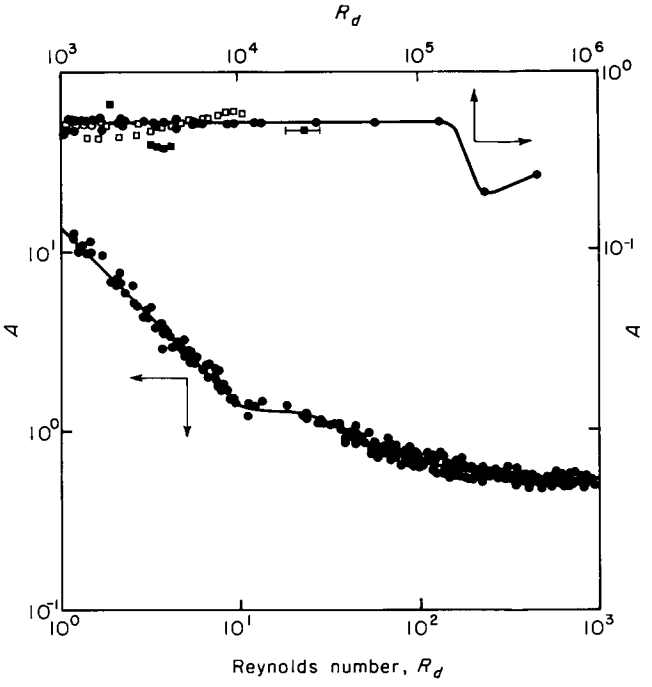

Figure 1 Reynolds number dependence of pressure loss factor A for SMR and PR grids. Symbols as given in Table 2. Curve fits: $R_d<10$, $A=14/R_d$; $40<R_d<10^5$, $A=0.52+66/R_d^{4/3}$

No Reynolds number dependence is found when using square-mesh arrays of square bars (SMS), at least for $10^2<R_d<10^4$. This is not surprising, since the location of flow separation would be expected to be fixed at the trailing edge corners. However, it is found that use of an exponent B other than 1 would be most suitable for this type of grid (see Fig 2). Although there are fewer data points, a definite trend is suggested, with $A=0.98$ and $B=1.09$[32,35,36,39].

For the parallel arrays of square bars (PS), only the present (limited) data are available. However, these data are seen to agree well with the SMS data (see Fig 2).

Finally, the perforated plate (PP) pressure losses are considered. Ref 40 suggests a rather complex formula for the pressure losses as a function of porosity β and the ratio of plate thickness to hole diameter, t/D, for the ranges $0<\beta<0.48$ and $1<t/D<7$. However, the present analysis of the available data suggests a much simpler functional relationship for $t/D\lesssim 0.2$ as shown in Fig 2, taken from Refs 24, 36, 39 and 41 and present work. The degree of scatter is reasonable, and it is suggested that Eq (1) can be used with confidence, putting $A=0.94$ and $B=1.28$. For t/D greater than 0.2, the 'constant' A is found to be a function of t/D which is well fitted by

$$A=0.94/(1+3(t/D)^4) \qquad (23)$$

in the range $0<t/D<0.8$ and $0.05<\beta<0.95$; see Ref 40 for further details.

Turbulence intensity

Streamwise component

Examination of the data available in the literature, together with the present results, suggests that the constant C in Eq (2) is independent of Reynolds number, at least in the range $10^2<R_d<10^4$; this is found to be the case for all grid types. From experiments with an SMR grid, however, Kistler and Vrebalovich[30] obtained data over the range $2.6\times10^4<R_d<45\times10^4$ and found a strong Reynolds number dependence. This is likely to be the same with PR grids, and is due to the rapidly changing aerodynamics at these transitional Reynolds numbers. The usual (subcritical Reynolds numbers) laminar separation from the wires/rods is replaced first by asymmetric separated flow, being somewhat erratic in nature, and eventually by fully turbulent flow separation at about $\pm120°$ to the main flow vector[42]. This transitional/supercritical Reynolds number regime is of little practical value in the usual turbulence grid applications, however, and is only mentioned here for completeness. Thus, as long as the grid is used in the Reynolds number range $10^2<R_d<10^4$ the following analysis should give satisfactory prediction.

For the SMR and PR grids, the available data are shown in Fig 3, taken from Refs 5, 35, 38, 43 to 59 and the present results. It is found that $C=0.80$ for both grid types. Clearly, there is some scatter in the results, but this is no doubt due to the

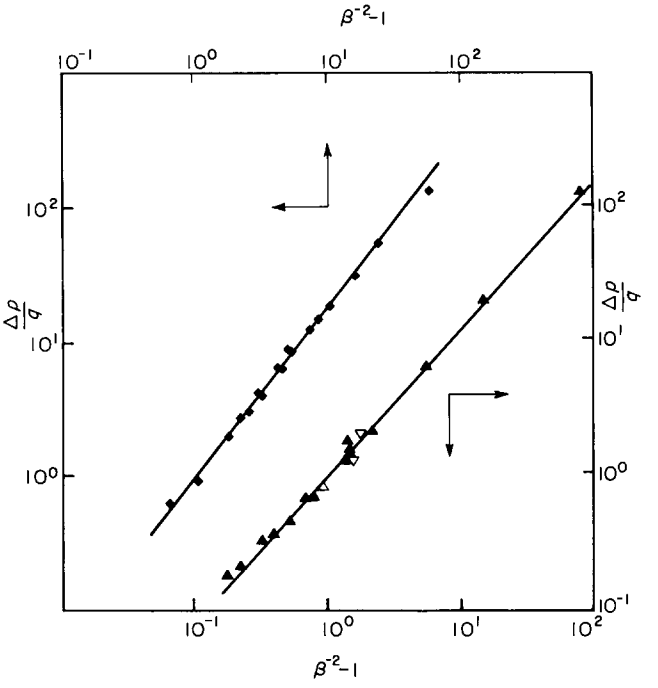

Figure 2 Pressure loss of SMS, PS and PP grids. Symbols as given in Table 2. Curve fits: SMS and PS grids, $\Delta p/q=0.98\ (\beta^{-2}-1)^{1.09}$; PP grids, $\Delta p/q=0.94(\beta^{-2}-1)^{1.28}$

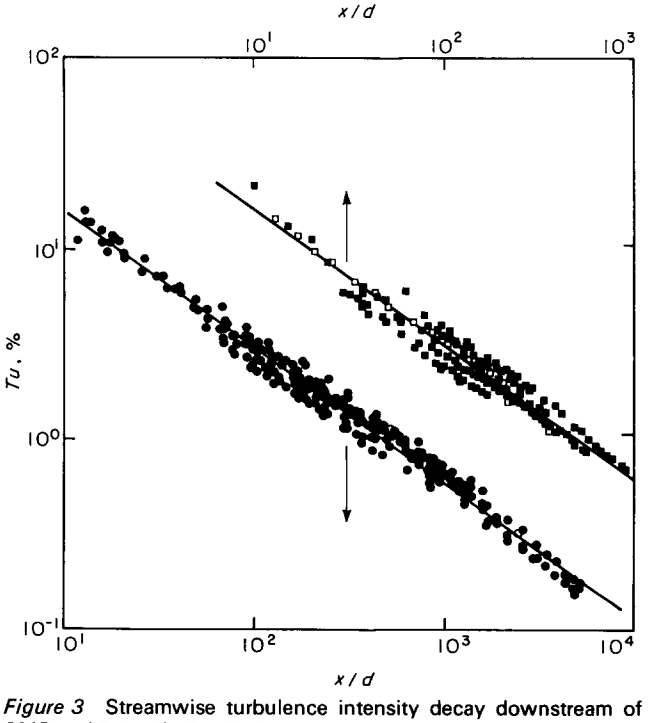

Figure 3 Streamwise turbulence intensity decay downstream of SMR and PR grids. Symbols as given in Table 2. Curve fits: SMR and PR grids, $Tu=0.80(x/d)^{-5/7}$

problems outlined in the literature review, above. Perhaps the most relevant problem which contributes to this scatter is the unsteady nature of flow separation from round wires/rods.

Results for the SMS grids are shown in Fig 4, taken from Refs 39, 46 and 60 to 65. The level of scatter is less than that with the SMR grids, which might be expected due to the fixed location of flow separation with the former type. The constant of proportionality, C, is found to be 1.13, very close to the value 1.12 given by Ref 39 in 1951.

This author has been unable to find many data sets from the use of PS grids; see Fig 4 (Refs 61, 66, 67 and present work). Moreover, what data there are appear contradictory. However, close examination shows that the ratio of grid mesh to wind tunnel width, M/W, was rather large for the Ref 61 data. Ref 66 gives only the curve fits to their data, and the higher of the two curves shown in Fig 4 was again obtained with a grid of rather large M/W. Moreover, Ref 61 does indicate that his PS grids produced rather 'unusual' spectra. Therefore, the lower set of data has been opted for by this author. This is in agreement with the SMS data, with the value of constant C of 1.13 agreeing well with these more limited data.

When using SMR or SMS grids, the question of whether or not there are differences in using biplanar, monoplanar or interwoven arrangements has frequently been addressed. Denoting the centre-to-centre streamwise spacing of grid elements by S, Ref 46 documents the turbulence properties of square bar and round rod arrays and finds no significant influence of spacing in the range $0 < s/d < 18.7$. In this case, the downstream position is relative to the trailing edge of the downstream grid elements. Ref 46 also reports that the degree of rectangularity of the bars used in a grid was insignificant for $0.5 < d/a < 4.0$ where a and d are the lengths of the sides in the streamwise and normal directions, respectively. In this case, the length scale used to render dimensionless the distance downstream of the grid is the side length normal to the flow vector, d.

Finally, the available data using PP grids are shown in Fig 5, taken from Refs 39, 68 to 70 and the present results. Using the equivalent diameter d_e given in Eq (22), the results are seen to be fitted fairly well by Eq (2) using the value 1.13 for the constant C: one would expect PP grids to behave more like the square bar

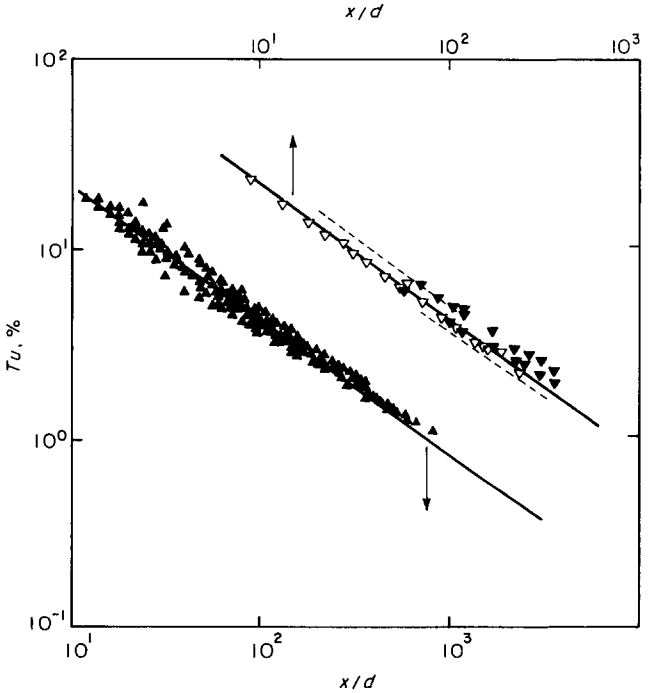

Figure 4 Streamwise turbulence intensity decay downstream of SMS and PS grids. Symbols as given in Table 2. Curve fits: SMS and PS grids, $Tu = 1.13(x/d)^{-5/7}$

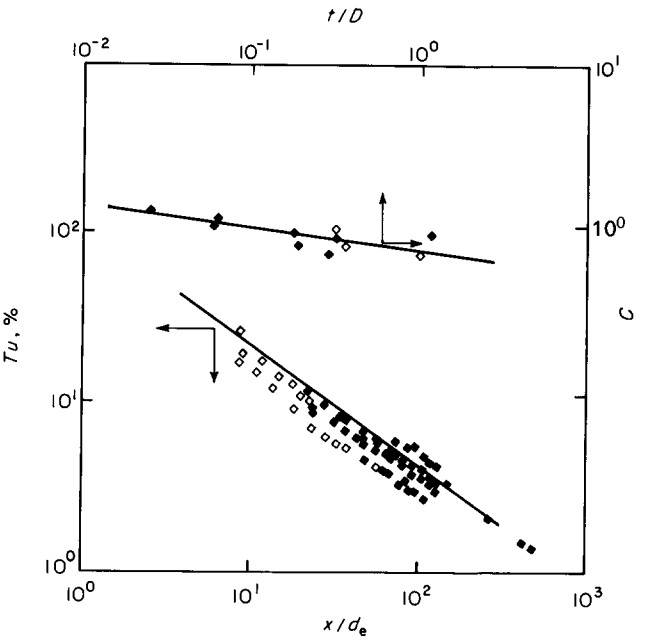

Figure 5 Streamwise turbulence intensity decay downstream of PP grids. Symbols as given in Table 2. Curve fits: $Tu = 1.13(x/d_e)^{-5/7}$; $C = 0.77(t/D)^{-0.14}$

grids than those with round rods. The level of scatter is rather high, and it is suggested this is due to the more complex flow separation phenomena using these grids. In fact, much better correlation can be obtained if C is assumed to be a function of the plate thickness to hole diameter ratio t/D (see Fig 5). Although the data are rather limited, the correlation is seen to be fairly good, suggesting

$$C = 0.77(t/D)^{-0.14} \tag{24}$$

Normal components

Examination of the available experimental findings regarding the normal components of turbulence indicates considerably more data scatter and a rather confused understanding. Generally speaking, it can be stated that the measured normal components of turbulence energy are equal and always less than the streamwise component. This difference diminishes slowly with increasing distance downstream, indicating a lack of self-preservation of the turbulence field. Results are available for SMR grids[30,47,58,59], PR grids[5,38], SMS grids[39,47,61,62,65] and PS grids[61,66]. A fair mean value for the ratio of turbulence energies $(\overline{u^2}/\overline{v^2})$ of 1.25 is indicated for all grid types, though individual experiments demonstrate that this ratio can take values anywhere in the range 1.0 to 1.5. It is this increased degree of uncertainty, obtained with grids of nominally the same geometric and aerodynamic parameters, which suggests that this ratio might be strongly influenced by the experimental apparatus or instrumentation used rather than the grid.

Now, nearly all of the available measurements have been made with a cross hot-wire probe of some description. As discussed fully in the Appendix, the yaw response of an inclined hot-wire element deviates from the expected cosine law by an amount which is primarily a function of probe geometry and angular orientation[15,17]. This deviation from the expected response leads to systematic errors in the measured fluctuating velocity components which can be quite significant, depending on the precise geometry of the probe. Moreover, the most widely used correction scheme leads to correction factors (k) for both $\overline{u^2}$ and $\overline{v^2}$ which are not equal, and suggest that the indicated (measured) value for the turbulence energy ratio $(\overline{u^2}/\overline{v^2})$ would be in the range 1.04 to 1.40, an average number being 1.17 if $k = 0.2$ (see the Appendix). This is in remarkable agreement with the turbulence energy ratio measured downstream of grids, as indicated above. For this reason, no further analysis of the

measurements of normal components of turbulence is attempted here.

Because of the agreement of the above figures, it is suspected that the measured anisotropy of grid turbulence is primarily a result of the measurement techniques used, and that grid turbulence is more nearly isotropic than has been believed for many years. Further support for this argument is given below.

Power spectra and correlation functions

Examples of one-dimensional power spectra and auto-correlations (taken from the present work) are shown in Figs 6 and 7. In these figures, f is the frequency and E is the power spectral density, rendered dimensionless by the mean velocity U, the streamwise turbulence energy $\overline{u^2}$, and the streamwise integral length scale. T is the time delay, and the autocorrelation function $R(T)$ is defined above. The 'analysis' curves are derived from Eqs (5) and (6). It must be noted that these formulae only apply to strictly homogeneous, isotropic turbulence in a uniform velocity flow field, and even then they do not apply for very high frequencies or very small time delays. Nevertheless, they are seen to agree remarkably well with the present results, suggesting that the generated turbulence is indeed very nearly isotropic.

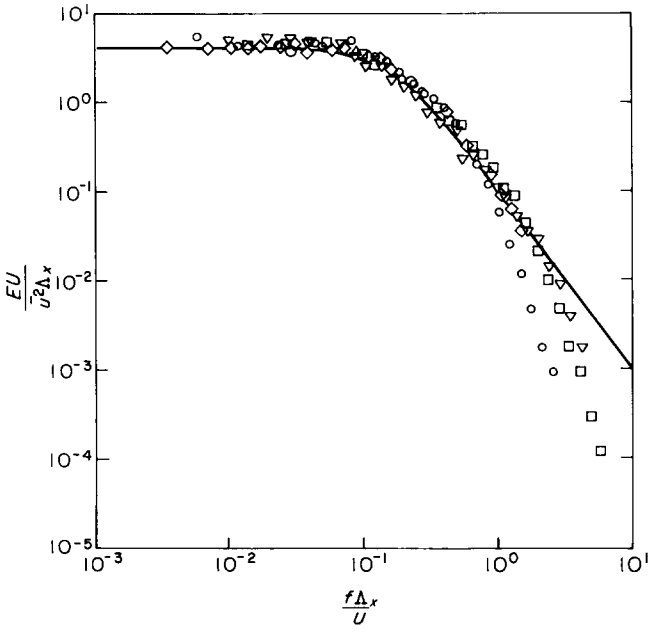

Figure 6 Spectral distribution of the axial turbulence component. Symbols as given in Table 2

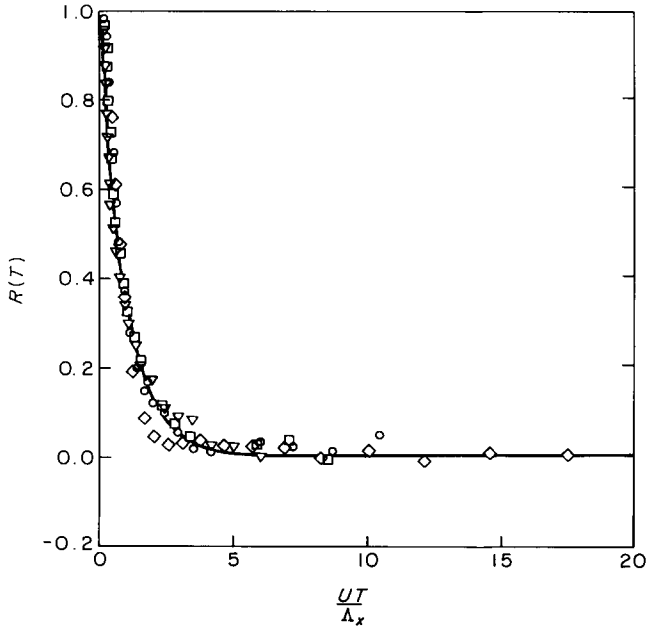

Figure 7 Autocorrelation of the axial turbulence component. Symbols as given in Table 2

Similarly good agreement between measured spectra and Eq (5) will be found in the literature. Moreover, examination of the present power spectra suggests that the analytical function deviates from the measured data at a fairly repeatable value of $f\Lambda_x/U \approx 2.0$. This limit also appears to be fairly well supported by available results in the literature.

Turbulence length scales

Both the integral and micro-scales of the turbulent flow field are found to be independent of grid type. At first, this might appear to be incredible, but one could imagine the turbulent eddies to scale primarily with the rod/bar dimension, whereas the turbulence energy is also a function of bar drag coefficient.

Measurements of streamwise and normal components of micro-scales are shown in Fig 8, taken from Refs 43 to 45, 55 to 59, 71 and the present work. From the available results it is seen that a suitable value for both F and G (Eqs (11) and (12)) is 1.21. Due to the absence of data, it seems sufficient to assume that $\lambda_z \equiv \lambda_y$, ie H (Eq (13)) is also 1.21. The equality of F and G implies that the turbulence field is truly isotropic, ie Eq (9) is correct. The fact that the constant F differs from unity would suggest that Eq (10) is not exact. This apparent discrepancy, which has been glossed over in the past, could be due to the measurement difficulties already discussed in the literature review in this paper. Nevertheless, the consistency of the results might be taken as an indication of their reliability, and it is recommended that the empirical constants F and G are taken to be correct. Further discussion is given in the Appendix.

Streamwise and normal component measurements of integral length scales are presented in Fig 9, taken from Refs 5, 43 to 46, 48, 55, 61, 62, 64, 65 and the present data. The increased level of scatter is due to the uncertainties in determining the integral scale, which can easily reach $\pm 10\%$. The data have been fitted by Eqs (18) and (19), with the constants I and J found to be 0.20 and 1.00, respectively, and one might assume with confidence

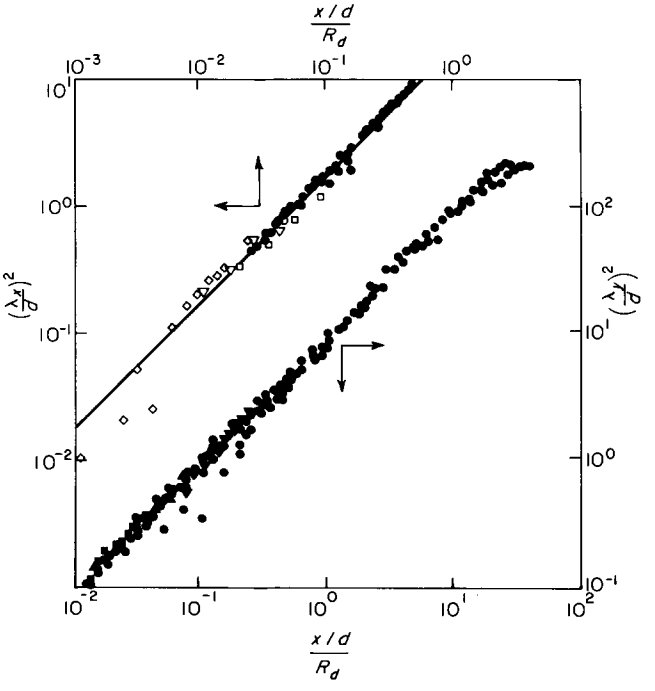

Figure 8 Micro-scale growth downstream of grids. Symbols as given in Table 2. Curve fits: $(\lambda_x/d)^2 = (17.0/R_d)(x/d)$; $(\lambda_y/d)^2 = (8.5/R_d)(x/d)$

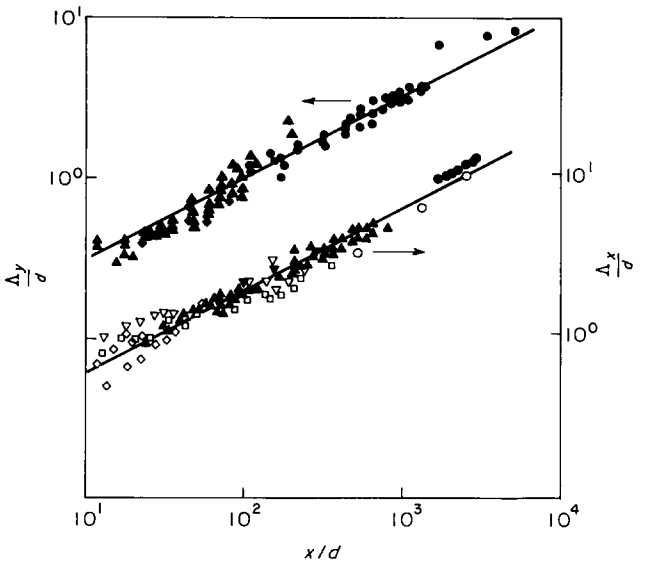

Figure 9 Integral scale growth downstream of grids. Symbols as given in Table 2. Curve fits: $\Lambda_x/d = 0.20(x/d)^{1/2}$; $\Lambda_y/d = 0.10(x/d)^{1/2}$

that $K = 1.00$ (Eq (20)). As with the micro-scales, the integral length scale data suggest a high degree of isotropy, albeit with a much greater data scatter. Several workers have found $\Lambda_x \approx 1.9\Lambda_y$. Nevertheless, in view of the large quantity of data in Fig 9 it is suggested that the figures quoted above can be used with confidence.

Concluding remarks

A parametric study of the aerodynamic characteristics of grids has been presented. Pressure losses, turbulence intensities and length scale data suggest a high degree of isotropy, albeit with a and aerodynamic parameters. Simple analyses have been used to correlate the experimental results and to aid in their understanding. The empirical 'constants' are summarized in Table 2; these are to be used with the appropriate equations given in the text.

The major conclusions are summarized below.

(a) Pressure losses are found to be primarily a function of grid solidity. Round rod/wire grids are also found to be strongly influenced by Reynolds number, but this is not the case with square bar grids and perforated plates.

(b) Grid generated turbulence intensity is found to decay with downstream distance at a rate proportional to $x^{-5/7}$. The turbulence energy scales on rod/bar dimensions rather than mesh size, and strongly reflects the bar drag coefficient. Turbulence energy measurements suggest that the generated flow field is markedly anisotropic; however, strong evidence is presented which suggests this is not the case, and that grid turbulence is more isotropic than has been believed for many years.

(c) Power spectra and correlation measurements support the view that the turbulence field is isotropic. Karman's one-dimensional spectrum is found to agree well with measurements, as is Dryden's exponential function for the correlation measurements.

(d) Eddy length scales are found to be independent of grid type, and scale primarily on the rod/bar dimension. Both micro and integral length scales are found to grow at a rate proportional to $x^{1/2}$ downstream of a grid. Micro-scales are also found to be a function of Reynolds number, as predicted. Length scale measurements indicate highly isotropic turbulent flow downstream of all grid types.

Acknowledgements

The author would like to thank Rolls-Royce plc for permission to publish this paper, and his colleagues at the Advanced Research Laboratory for their contributions. Thanks are also due to numerous researchers in this country and abroad who have been so willing to impart advice and experimental data. This work was financially supported by the Ministry of Defence.

References

1 Loehrke, R. I. and Nagib, H. M. Experiments on management of free-stream turbulence, AGARD-R-598, 1972
2 Laws, E. M. and Livesey, J. L. Flow through screens. *Ann. Rev. Fluid Mech.*, 1978, **10**, 247–266
3 Kiock, R. Influence of the degree of turbulence on the aerodynamic coefficients of cascades, AGARD-AG-164, 1972
4 Ling, S. C. and Wan, C. A. Decay of isotropic turbulence generated by a mechanically agitated grid. *Phys. Fluids*, 1972, **15**(8), 1363–1369
5 Gad-el-Hak, M. and Corrsin, S. Measurements of the nearly isotropic turbulence behind a uniform jet grid. *J. Fluid Mech.*, 1974, **62**(1), 115–145
6 Tassa, Y. and Kamotani, Y. Experiments on turbulence behind a grid with jet injection in downstream and upstream direction. *Phys. Fluids*, 1975, **18**(4), 411–414
7 Evans, R. L. Turbulence and unsteadiness measurements downstream of a moving blade row. *Trans. ASME*, 1975, *J. Eng. Power* 131–139
8 Kiock, R. Turbulence downstream of stationary and rotating cascades, ASME Paper 73-GT-80, 1973
9 Lakshminarayana, B. and Davino, R. Mean velocity and decay characteristics of the guidevane and stator blade wake of an axial flow compressor. *Trans. ASME*, 1980, *J. Eng. Power*, **102**, 50–60
10 Roach, P. E. The generation of nearly isotropic turbulence downstream of streamwise tube bundles. *Int. J. Heat Fluid Flow*, 1986, **7**(2), 117–125
11 Hoerner, S. F. *Fluid dynamic drag*, published by author, 1958
12 Schlichting, H. *Boundary layer theory*, McGraw-Hill, 6th edn, 1968
13 Roach, P. E. The aerodynamic performance of short struts immersed in end-wall boundary layers, PhD Thesis, University of Manchester, 1982
14 Bradshaw, P. *An introduction to turbulence and its measurement*, Pergamon Press, 1971
15 Hinze, J. O. *Turbulence*, McGraw-Hill, 1st edn, 1959
16 Derksen, R. W. and Azad, R. S. An examination of hot-wire length corrections. *Phys. Fluids*, 1983, **26**(7), 1751–1754
17 Vagt, J. D. Hot-wire probes in low speed flow. *Prog Aerospace Sci.*, 1979, **18**(4), 271–323
18 Pinker, R. A. and Herbert, M. V. Pressure loss associated with compressible flow through square-mesh wire gauzes. *J. Mech. Eng. Sci.*, 1967, **9**(1), 11–23
19 —— Pressure drop in ducts across round-wire gauzes normal to the flow, ESDU 72009, 1972
20 Batchelor, G. K. *The theory of homogeneous turbulence*, Cambridge University Press, 1967
21 Frenkiel, F. N. The decay of isotropic turbulence. *Trans. ASME*, 1948, *J. Appl. Mech.*, 311–321
22 Naudascher, E. and Farell, C. Unified analysis of grid turbulence. *Proc. ASCE*, 1970, *J. Eng. Mech. Div.*, **EM2**, 121–141
23 Bernardi, R. T., Linehan, J. H. and Hamilton, L. H. Low Reynolds number loss coefficient for fine-mesh screens. *Trans. ASME*, 1976, *J. Fluids Eng.*, 762–764
24 Collar, A. R. The effect of a gauze on the velocity distribution in a uniform duct, ARC R&M 1867, 1939
25 Crane, J. F. W. The use of woollen felt screens as air cleaners for supersonic wind tunnels, ARC CP538, 1960
26 Dryden, H. E. and Schubauer, G. B. The use of damping screens for the reduction of wind-tunnel turbulence. *J. Aerospace Sci.*, 1947, 221–228
27 Eckert, B. and Pflüger, F. The resistance coefficient of commercial round-wire grids, NACA TM1003, 1942
28 Gibson, M. M. The design and performance of a streamline diffuser with a rapid expansion, ARC 21126, FM 2843, 1959
29 Grootenhuis, P. A correlation of the resistance to airflow of wire gauzes. *Proc. Inst. Mech. Engrs.*, 1954, **68**(34), 837–846

30 Kistler, A. L. and Vrebalovich, T. Grid turbulence at large Reynolds numbers. *J. Fluid Mech.*, 1966, **26**(1), 37–47
31 Morgan, P. G. High speed flow through wire guzes. *J. R. Aero. Soc.*, 1959, **63**, 474–477
32 Morgan, P. G. Fluid flow through screens of low solidity. *J. R. Aero. Soc.*, 1962, **66**, 54–56
33 Schubauer, G. B., Spangenberg, W. G. and Klebanoff, P. S. Aerodynamic characteristics of damping screens, NACA TN 2001, 1950
34 Simmons, L. F. G. and Cowdrey, C. F. Measurements of the aerodynamic forces acting on porous screens, ARC R&M 2276, 1945
35 Symes, C. R. and Fink, L. E. Effects of external turbulence upon the flow past cylinders. In: *Structure and mechanisms of turbulence I*, 1977, **75**, 86–102
36 Taylor, G. I. and Davies, R. M. The aerodynamics of porous sheets, ARC R&M 2237, 1944
37 Wieghardt, K. E. G. On the resistance of screens. *Aero Q.*, 1953, **4**, 186–192
38 Harris, V. G. The turbulence generated by an array of parallel rods, MSc Thesis, Johns Hopkins University, Baltimore, 1965
39 Baines, W. D. and Peterson, E. G. An investigation of flow through screens. *Trans. ASME*, 1951, 467–480
40 —— Pressure losses across perforated plates, orifice plates and cylindrical tube orifices in ducts, ESDU 72010, 1972
41 Ward-Smith, A. J. *Pressure losses in ducted flows*, Butterworths, London, 1971
42 Bearman, P. W. The flow around a circular cylinder in the critical Reynolds number regime, NPL Aero. Rpt. 1273, 1968
43 Batchelor, G. K. and Townsend, A. A. Decay of isotropic turbulence in the initial period. *Proc. R. Soc.*, 1948, *A*, **193**, 539–558
44 Batchelor, G. K. and Townsend, A. A. Decay of isotropic turbulence in the final period. *Proc. R. Soc.*, 1948, *A*, **194**, 527–543
45 Bennet, J. C. and Corrsin, S. Small Reynolds number nearly isotropic turbulence in a straight duct and a contraction. *Phys. Fluids*, 1978, **21**(12), 2129–2140
46 Charnay, G., Comte-Bellot, G. and Mathieu, J. Development of a turbulent boundary layer on a flat plate in an external turbulent flow. *AGARD CP*93, 1971, *paper* 27
47 Comte-Bellot, G. and Corrsin, S. The use of a contraction to improve the isotropy of grid-generated turbulence. *J. Fluid Mech.*, 1966, **25**(4), 657–682
48 Hall, A. A. Measurements of the intensity and scale of turbulence, ARC R&M 1842, 1938
49 Karman, T. von. Some remarks on the statistical theory of turbulence. *Proc. 5th Int. Cong. Appl. Mech.*, 1938, 347–351
50 Kline, S. J., Lisin, A. V. and Waitman, B. A. Preliminary experimental investigation of effect of free-stream turbulence on turbulent boundary layer growth, NASA TND 368, 1960
51 Robertson, J. M. and Holt, C. P. Stream turbulence effects on turbulent boundary layer. *Proc. ASCE*, 1972, *J. Hyd. Div.*, **98**(HY6), 1095–1099
52 Evans, R. L. Stream turbulence effects on the turbulent profile boundary layer in a compressor cascade, ARC 34587, 1973, Turbo. 267; CUED/A Turbo/TR 43
53 Sadeh, W. Z. and Sullivan, P. P. Turbulence amplification in flow about an airfoil, ASME 80-GT-111, 1980
54 Huffman, G. D., Zimmerman, D. R. and Bennet, W. A. The effect of free-stream turbulence level on turbulent boundary layer behaviour, AGARD AG164, 1972
55 Stewart, R. W. and Townsend, A. A. Similarity and self-preservation in isotropic turbulence. *Phil. Trans. R. Soc.*, 1951, *A*, 867, **243**, 359–386
56 Tsuji, H. and Hama, F. R. Experiment on the decay of turbulence behind two grids. *J. Aero. Sci.*, 1953, **20**, 848–849
57 Uberoi, M. S. and Wallis, S. Effect of grid geometry on turbulence decay. *Phys. Fluids*, 1967, **10**(6), 1216–1224
58 Venkataramani, K. S. and Chevray, R. Statistical features of heat transfer in grid generated turbulence: constant gradient case. *J. Fluid Mech.*, 1978, **86**(3), 513–543
59 Wyatt, L. A. Energy and spectra in decaying homogeneous turbulence, PhD Thesis, University of Manchester, 1955
60 Castro, I. P. Effects of free-stream turbulence on low Reynolds number boundary layers. *Trans. ASME*, 1984, *J. Fluids Eng.*, **106**, 298–306
61 Hancock, P. E. The effect of free-stream turbulence on turbulent boundary layers, PhD Thesis, Imperial University, 1980
62 Nakamura, Y. and Ohya, Y. The effects of turbulence on the mean flow past square rods. *J. Fluid Mech.*, 1983, **137**, 331–345
63 Sato, H. Experimental study of the spectrum of isotropic turbulence. I. *J. Phys. Soc. Japan*, 1951, **6**(5), 387–392
64 Sirivat, A. and Warhaft, Z. The mixing of passive helium and temperature fluctuations in grid turbulence. *J. Fluid Mech.*, 1982, **120**, 475–504
65 Sirivat, A. and Warhaft, Z. The effect of a passive cross-stream temperature gradient on the evolution of temperature variance and heat flux in grid turbulence. *J. Fluid Mech.*, 1983, **128**, 323–346
66 Veeravalli, S. and Warhaft, Z. The interaction of two distinct turbulent velocity scales in the absence of mean shear. *5th Symp. Turb. Shear Flows*, 1985, **15**, 11–15.17
67 Gilbert, B. Diffusion mixing in grid turbulence without mean shear. *J. Fluid Mech.*, 1980, **100**, 349–365
68 Kadotani, K. and Goldstein, R. J. On the nature of jets entering a turbulent flow—Part A: Jet–mainstream interaction. JSME/GTSJ/ASME Joint Gas Turbine Congress, Tokyo, 1977
69 Came, P. M. A turbulence grid for a cascade tunnel, NGTE TURBO 894, 1967, unpublished
70 Gilbert, B. Turbulent flows produced by perforated plate generators in wind tunnels. *AIAA J.*, 1980, **13**(3)
71 Uberoi, M. S. and Wallis, S. Spectra of grid turbulence. *Phys. Fluids*, 1969, **12**(7), 1355–1358
72 Bruun, H. H. and Tropea, C. The calibration of inclined hot-wire probes. *J. Phys, E: Sci. Instrum.*, 1985, **18**, 405–413

Appendix—Yaw sensitivity of crossed hot-wire probes

When using an inclined hot-wire probe of 'infinite' length, the heat transfer depends only on the component of velocity normal to the wire axis. For any finite length of wire this can be only a first approximation, which is only good at low angles ($<10°$) between the wire normal and the mean flow direction. This approximation breaks down, however, at larger inclination angles, when the component of velocity parallel to the wire has a significant influence on the wire characteristics. Considering the most common correction scheme[17] it is found that the effective cooling velocity U_e is given by

$$U_e^2 = U^2(\cos^2\alpha + k^2\sin^2\alpha) \tag{A.1}$$

where U is the true velocity, α is the wire inclination angle (yaw), and k is the correction factor which must be determined experimentally for each wire. Following the analysis of Ref 17, the necessary corrections to the measured turbulence energies can be determined. For linearized operation, these quantities are given by

$$(\overline{u^2})_m = (1+k^2)(\overline{u^2})_t \tag{A.2}$$

$$(\overline{v^2})_m = \frac{(1-k^2)^2}{(1+k^2)}(\overline{v^2})_t \tag{A.3}$$

where $\overline{u^2}$ and $\overline{v^2}$ are the streamwise and normal turbulence energy, respectively, and the subscripts m and t denote measured and true values. It is assumed here that the 'measured' values are obtained by only accounting for the velocity component normal to the wire axis, ie putting $k=0$.

This correction factor k has been determined by numerous workers, with an average figure of 0.2 being found, though figures between 0.1 and 0.3 (or more) are found in practice, depending on the precise geometry of the probe. Assuming the turbulence field is truly isotropic (ie $(\overline{u^2})_t \equiv (\overline{v^2})_t$), then Eqs (A.2) and (A.3) can be combined to give

$$\left(\frac{\overline{u^2}}{\overline{v^2}}\right)_m = \left(\frac{1+k^2}{1-k^2}\right)^2 \tag{A.4}$$

For $k=0.2$, $(\overline{u^2}/\overline{v^2})_m = 1.17$, though over the range $0.1<k<0.3$, $1.04<(\overline{u^2}/\overline{v^2})<1.43$. Clearly, these figures are not insignificant.

Now, similar formulae can be derived for the length scale measurements. Relating the streamwise components of fluctuating velocity with the corresponding length scales, and

doing likewise with the normal components, then from Eqs (2), (3), (11), (12), (18) and (19):

$$\left(\frac{\lambda_x}{\lambda_y}\right)_m = \left(\frac{\lambda_x}{\lambda_y}\right)_t \left[\left(\frac{Tu}{Tv}\right)_m \left(\frac{Tv}{Tu}\right)_t\right]^{-7/10}$$

$$\left(\frac{\Lambda_x}{\Lambda_y}\right)_m = \left(\frac{\Lambda_x}{\Lambda_y}\right)_t \left[\left(\frac{Tu}{Tv}\right)_m \left(\frac{Tv}{Tu}\right)_t\right]^{-7/10}$$

Now, for truly isotropic turbulence[15], $(\lambda_x/\lambda_y)_t = \sqrt{2}$, $(\Lambda_x/\Lambda_y)_t = 2$ and $(Tu/Tv)_t = 1$. Substitution of these figures, and combining with Eq (A.4), gives

$$\left(\frac{\lambda_x}{\lambda_y}\right)_m = \sqrt{2}\left(\frac{1+k^2}{1-k^2}\right)^{-7/10} \quad \text{(A.5)}$$

$$\left(\frac{\Lambda_x}{\Lambda_y}\right)_m = 2\left(\frac{1+k^2}{1-k^2}\right)^{-7/10} \quad \text{(A.6)}$$

Using the typical value of $k = 0.2$ gives $(\lambda_x/\lambda_y)_m = 1.34$ and $(\Lambda_x/\Lambda_y)_m = 1.89$. Over the usual range $0.1 < k < 0.3$:

$1.39 > (\lambda_x/\lambda_y)_m > 1.25, \qquad 1.97 > (\Lambda_x/\Lambda_y)_m > 1.76.$

As a test of the validity of Eq (A.4), a brief series of experiments was undertaken in the wind-tunnel, using the grids described in Table 1. The results of this work are shown in Table A.1, where it has been assumed that $k = 0$, and $10 < U < 20$ m/s.

Table A.1

Grid type	$\frac{x}{d}$	$\left(\frac{\overline{u^2}}{\overline{v^2}}\right)$
SMR	515	1.07
		1.13
PR	74	1.08
		1.10
		1.06
PS	49	1.09
		1.10
		1.09

A standard DISA P53 x-wire probe was used to obtain the above data, and over the flow velocity range under investigation, the k-factor was experimentally determined to be 0.14 (compare with Ref 72). From Eq (A.4) it is seen that (for truly isotropic turbulence) the expected measured ratio of turbulence energies (ignoring the k-factor) would therefore be 1.08. This latter figure is in remarkable agreement with the figures given in Table A.1, which shows an average figure of 1.09 for $(\overline{u^2}/\overline{v^2})$. Although these rather limited data do not prove that grid turbulence is truly isotropic, the very close agreement of the above figures strongly suggests that it is, at least to within experimental uncertainty.

Book review

The chemical engineering guide to heat transfer

Ed. K. J. McNaughton

This two-volume set is a collection of reprints from *Chemical Engineering* magazine. The reprinted articles date from 1979 to 1985 and cover a very wide range of heat transfer topics including basic equipment such as fired heaters, boilers, refrigeration systems, cooling towers, agitated vessels and dryers. More exotic subjects addressed include heat pipes, hydraulic turbines, solar ponds and microwave dryers. There are also topics which some heat transfer engineers might regard as 'gatecrashers' namely steam traps, steam tracing and insulation.

The main emphasis, however, is on heat exchangers and, especially, shell and tube heat exchangers.

The two substantial, well printed, solidly bound, quarto sized volumes are entitled respectively 'Plant Principles' and 'Equipment', titles which are rather vague and, as it turns out, somewhat irelevant as regards the contents. However, the amount of material is too large for one volume and I suppose the editor had to find a title of some sort for each of the resulting two. Classifying such a large and diverse range of articles must, in fact, be quite a difficult task but classify them he does, fairly successfully, under six headings in each volume namely, Heat Exchangers, Shell & Tube Equipment, Design, Heat Recovery, Steam and Cost and, in volume 2, Boilers, Cooling, Heating & Insulation, Condensers, Dryers and Other Equipment.

Those familiar with 'Chemical Engineer' magazine will know that it specializes in articles of an intensely practical nature written by practising engineers who are anxious to share many years of hard, and often painful, experience with colleagues. Prospective readers looking for good heat transfer science will, therefore, be disappointed. Indeed, the articles in this collection which fall down flattest are those where the authors are attempting to be at their most scientific. Examples of this include several articles on calculating multipass log mean temperature difference which are largely taken up by the tedious algebra found in many standard texts.

Sympathy, however, must be extended to the many Hewlett Packard HP-67 buffs contributing to the book who laboured long and hard programming up thermal design methods from Kern and others only to find their efforts overtaken by the mid-eighties generation of personal computers and associated sophisticated software.

Where the books really do score, however, is in the collected experience of specialists who, over the years, have had to select, design, buy, construct, operate and troubleshoot all kinds of heat exchangers and other equipment. Much of this hands-on experience is never written down except in magazine articles and is most unlikely to be found in the more academic texts.

Also hard to find elsewhere and very useful are the articles on cost estimation. Although the information contained in these is now a few years out of date the application of a judicious factor to account for recent, mercifully small, rises in costs should render these estimation methods still very helpful.

This one is, then, very much for the practising engineer in the oil and gas industry and probably more for the operating company generalist rather than the contracting/manufacturing specialist.

Chris Norman
Harwell Laboratory,
Oxfordshire, England

Published price $49.50 by Hemisphere Publishing Corporation, 79 Madison Ave, New York, NY 10016, USA, 300 pp.